IEEE Photonics Journal
An IEEE Photonics Society Publication

Open Access

Joint Noise Reduction for Contrast Enhancement in Stokes Polarimetric Imaging

Volume 11, Number 2, April 2019

Hui Wang
Haofeng Hu
Xiaobo Li
Lin Zhao
Zijian Guan
Wanshan Zhu
Junfeng Jiang
Kun Liu
Zhenzhou Cheng
Tiegen Liu

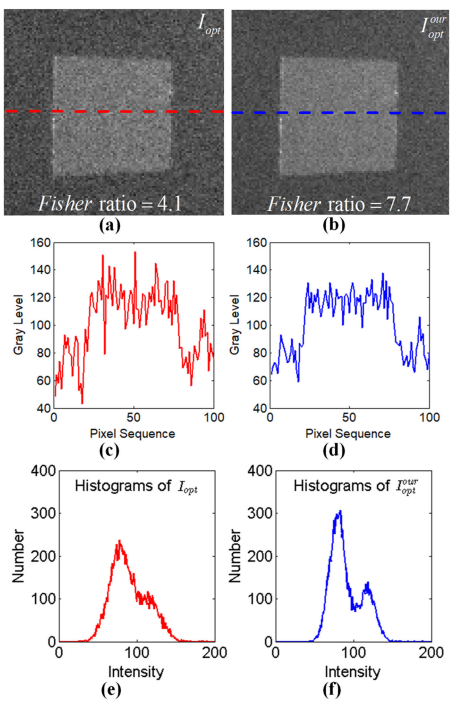

DOI: 10.1109/JPHOT.2019.2902256

Joint Noise Reduction for Contrast Enhancement in Stokes Polarimetric Imaging

Hui Wang,[1,2,3,4] **Haofeng Hu**,[1,2,3,5] **Xiaobo Li**,[1,2,3] **Lin Zhao**,[1,2,3] **Zijian Guan**,[1,2,3] **Wanshan Zhu**,[1,2,3] **Junfeng Jiang**,[1,2,3] **Kun Liu**,[1,2,3] **Zhenzhou Cheng**,[1,2,3] **and Tiegen Liu**[1,2,3,5]

[1]School of Precision Instrument & Opto-electronics Engineering, Tianjin University, Tianjin 300072, China
[2]Key Laboratory of Opto-electronics Information Technology, Ministry of Education, Tianjin 300072, China
[3]Tianjin Optical Fiber Sensing Engineering Center, Institute of Optical Fiber Sensing, Tianjin University, Tianjin 300072, China
[4]College of Physics Science and Information Engineering, Hebei Advanced Thin Films Laboratory, Hebei Normal University, Shijiazhuang 050024, China
[5]Joint Laboratory for Ocean Observation and Detection, Qingdao National Laboratory for Marine Science and Technology, Qingdao 266237, China

DOI:10.1109/JPHOT.2019.2902256

Manuscript received February 1, 2019; revised February 18, 2019; accepted February 24, 2019. Date of publication March 13, 2019; date of current version March 21, 2019. This work was supported in part by the National Natural Science Foundation of China under Grant 61775163, in part by Director Fund of Qingdao National Laboratory for Marine Science and Technology under Grant QNLM201717, in part by Young Elite Scientists Sponsorship Program by CAST under Grant 2017QNRC001, in part by National Instrumentation Program under Grant 2013YQ030915, and in part by China Postdoctoral Science Foundation under Grant 2016M601260. Corresponding author: Haofeng Hu (e-mail: haofeng_hu@tju.edu.cn).

Abstract: Contrast optimization is a key issue in polarimetric imaging for the purpose of target detection. In practice, the noise could induce the intensity fluctuation of the image and thus lead to the decrease of the image contrast. A joint noise reduction method is proposed for contrast enhancement in Stokes polarimetric imaging. The proposed method is based on the relation of the joint polarimetric image set, which includes four images taken to calculate Stokes vector and one image taken at the optimal state of a polarization state analyzer (PSA). By our method, the traditional contrast-enhanced image is modified to decrease the disturbance of noise, and the contrast of the image is further enhanced. Both the theoretical analysis and the real-world experimental results demonstrate that our method can effectively decrease the disturbance by the noise and thus increase the contrast of the image. In particular, it is found that the effect of the proposed method is independent of the optimal PSA state when the regular tetrahedron measurement matrix is implemented.

Index Terms: Polarimetric imaging, contrast enhancement, denoising.

1. Introduction

Polarimetric imaging is emerging as an attractive vision technique in remote sensing [1]–[3], machine vision [4]–[6], biomedical imaging [7]–[9] and underwater imaging [10]–[12]. It can reveal important information about the physical and geometrical properties which can not be obtained

from intensity or spectral images. Target detection is one of the most important aim of adopting polarimetric imaging, in which the key issues are improving the target/background contrast and reducing the noise disturbance [13]–[17].

In recent years, attention has been drawn on the strategy for contrast enhancement of polarimetric image. Contrast enhancement can be realized by different ways such as device design modification [2], parameter optimization [10], arithmetic improving [12] etc. In particular, Anna *et al*. [18] proposed an adaptive polarimetric imager which can be fully tunable for contrast enhancement. Goudail *et al*. [19] found that the image contrast provided by the adaptive system is always superior to the static one. By adaptive polarimetric imager, the contrast can be significantly enhanced by matching the polarization state analyzer (PSA) to the optimal state [20], [21]. The optimal PSA state is deduced by the Stokes vector that is obtained by four intensity images taken at four different PSA states [22]. It is worth noting that the four images are discarded after Stokes vector measurement in previous methods. Indeed, because the optimal image and the four images are taken for the same scene, there is a joint relation between them. We believe if we can take into account of the joint relation of these images, the contrast of image can be further improved.

We consider in this paper the configuration of Stokes polarimetric imaging. The traditional strategy of contrast optimization for Stokes polarimetric imaging involves three steps: 1) measuring the polarimetric information (Stokes vector) of the scene by taking four intensity images at four different states of PSA; 2) finding the optimal states for PSA according to the measured polarimetric information; 3) adjusting PSA to the optimal state, and outputting the polarimetric image with optimal contrast. Thus, there are five polarimetric images in the whole process of measurement. Combining images to reduce noise has been used in many fields, such as optical imaging [23] and medical inspection [24], [25]. However, with regard to the parametric images obtained by Stokes polarimetric imager, the problem is different from the previous ones. The five polarimetric images are joint physically. In this work, we investigate the joint relation between these five polarimetric images, and based on the joint relation of them, a new method is proposed to generate the modified polarimetric image in the presence of additive Gaussian noise. We show through analytical analysis and real-world experiments that the variance of the image induced by the noise can be considerably decreased and thus the contrast and the quality of the image can be further improved by our method.

2. Principle of Stokes Polarimetric Imaging

In Stokes polarimetric imaging system, the traditional method of optimizing contrast is realized by adjusting the state of PSA to maximize the intensity difference between target and background region. In this case, the measurement of polarization state of the scenes is necessary for deducing the optimal state of PSA. The polarization state of the light is expressed by the Stokes vector $\mathbf{S} = (S_0, S_1, S_2, S_3)^T$, where the superscript T denotes matrix transposition [26]. To obtain the full Stokes vector, one needs to measure at least four intensity images at different states of PSA [27]:

$$\mathbf{I}^{NN} = \frac{1}{2}\begin{pmatrix}\mathbf{T}_1^T\\ \mathbf{T}_2^T\\ \mathbf{T}_3^T\\ \mathbf{T}_4^T\end{pmatrix}\mathbf{S} = \frac{1}{2}\begin{pmatrix}1 & t_{11} & t_{12} & t_{13}\\ 1 & t_{21} & t_{22} & t_{23}\\ 1 & t_{31} & t_{32} & t_{33}\\ 1 & t_{41} & t_{42} & t_{43}\end{pmatrix}\begin{pmatrix}S_0\\ S_1\\ S_2\\ S_3\end{pmatrix} = W\mathbf{S}, \tag{1}$$

where $\mathbf{I}^{NN} = (i_1^{NN}, i_2^{NN}, i_3^{NN}, i_4^{NN})^T$ is the intensity vector that consist of four intensity with no noise (NN). W is the 4×4 measurement matrix of PSA composed by four eigenstates of PSA denoted by $\mathbf{T}_k = (1, t_{k1}, t_{k2}, t_{k3})^T$, $k = (1, 2, 3, 4)$. The Stokes vector can be retrieved from $\mathbf{I}^{NN}$ by inverting Eq. (1):

$$\mathbf{S} = W^{-1}\mathbf{I}^{NN}. \tag{2}$$

According to the measured Stokes vector, one can deduce the optimal state of PSA $\mathbf{T}_{opt}$ to maximize the contrast of the image [19]. When PSA is adjusted to the optimal state $\mathbf{T}_{opt}$, one can capture the image with the optimal contrast image as:

$$i_{opt}^{NN} = \frac{1}{2}\mathbf{T}_{opt}^{T}\mathbf{S}, \tag{3}$$

where i_{opt}^{NN} represents contrast-optimized image with no noise. However, noise is inevitable in practice and it will result in the reduction of image contrast. Therefore, reducing the effect of random noise is important for improving the contrast of image, especially in the condition of low light level. When noise is taken into account, Fisher ratio is a reasonable criterion for characterizing the discrimination ability between target *a* and background *b* [28], which is defined as:

$$F(i) = \frac{(\langle i_a \rangle - \langle i_b \rangle)^2}{\mathrm{Var}[i_a] + \mathrm{Var}[i_b]}, \tag{4}$$

where $\langle i_k \rangle$ and $\mathrm{Var}[i_k]$, $k = (a, b)$ refer to the mean value and variance of the intensity in target and background regions. A higher value of fisher ratio indicates a higher contrast of image. Our objective is to maximize fisher ratio of the image, and therefore, decreasing the variance of the image is the critical issue according to Eq. (4).

We assume that the noise of images is additive Gaussian which is frequently encountered in optical imaging systems [29]. The intensity image captured by CCD is expressed as:

$$\mathbf{I} = W\mathbf{S} + \mathbf{N}, \tag{5}$$

$\mathbf{I}$ is intensity vector $(i_1, i_2, i_3, i_4)^T$ indicating the four intensity images measured by polarimetric imaging system with measurement matrix W. $\mathbf{N}$ is noise vector $(n_1, n_2, n_3, n_4)^T$ indicating the noise of the corresponding intensity image. The noise leads to the variation of $i_k (k = 1, 2, 3, 4)$ with the variance same to σ^2 in the statistical sense. It needs to be noticed that the noise in each intensity measurement is independent from each other, and the statistical variation of each intensity i_k does not depend on the state of PSA and the Stokes vector to be measured. Therefore, the fifth image captured at the optimal PSA state $\mathbf{T}_{opt}$ is

$$i_{opt} = \frac{1}{2}\mathbf{T}_{opt}^{T}\mathbf{S} + n_5, \tag{6}$$

where n_5 is the noise of image i_{opt} with the variance of σ^2.

3. The Method of Polarimetric Joint Noise Reduction for Contrast Enhancement

As mentioned in the previous section, the Stokes vector is obtained through the four measurement images, and the optimal PSA state $\mathbf{T}_{opt}$ is determined to obtain a contrast-optimized image. These five intensity images can be considered as an over-complete set for Stokes vector measurement. Since the intensity image captured by CCD can be considered as a linear projection of Stokes vector, and there are linear relations between them. In particular, the fifth image can be expressed by the linear combination of other four images. According to Eq. (2) and Eq. (3), one can get

$$i_{opt}^{NN} = \frac{1}{2}\mathbf{T}_{opt}^{T}W^{-1}\mathbf{I}^{NN} = C\mathbf{I}^{NN} = c_1 i_1^{NN} + c_2 i_2^{NN} + c_3 i_3^{NN} + c_4 i_4^{NN}, \tag{7}$$

$$C = (c_1, c_2, c_3, c_4) = \frac{1}{2}\mathbf{T}_{opt}^{T}W^{-1}, \tag{8}$$

where C is a 1×4 matrix composed of the four weights of the linear transformation given by Eq. (7). By replacing $\mathbf{I}^{NN}$ in Eq. (7) with the measured intensity vector $\mathbf{I}$ given by Eq. (5), we construct a new random variable, which we call the composite image

$$i_{opt}^{com} = C\mathbf{I}, \tag{9}$$

where i_{opt}^{com} is a linear combination of $i_k (k = 1, 2, 3, 4)$ and i_k follows Gaussian distribution. Thus i_{opt}^{com} follows Gaussian distribution too. The mean value and variance of i_{opt}^{com} are:

$$\begin{cases} \langle i_{opt}^{com} \rangle = i_{opt}^{NN} \\ \mathrm{Var}[i_{opt}^{com}] = \|C\|^2 \sigma^2 \end{cases}, \tag{10}$$

where $\|C\| = \sqrt{CC^T}$ refers to the Euclidian norm of C. For a certain measurement, the probability that the value i_{opt}^{com} emerges in experiment is:

$$P(i_{opt}^{com}) = \frac{1}{\sqrt{2\pi}\,\|C\|\,\sigma} \exp\left[-\frac{\left(i_{opt}^{com} - i_{opt}^{NN}\right)^2}{2\,\|C\|^2\,\sigma^2} \right]. \tag{11}$$

On the other hand, according to Eq. (6), i_{opt} also follows Gaussian distribution, and thus we have:

$$\begin{cases} \langle i_{opt} \rangle = i_{opt}^{NN} \\ \mathrm{Var}[i_{opt}] = \sigma^2 \end{cases}. \tag{12}$$

The probability that i_{opt} emerges in experiment is:

$$P(i_{opt}) = \frac{1}{\sqrt{2\pi}\sigma} \exp\left[-\frac{\left(i_{opt} - i_{opt}^{NN}\right)^2}{2\sigma^2} \right]. \tag{13}$$

i_{opt}^{com} is deduced by the previous four images (i_1, i_2, i_3, i_4) according to Eq. (9), and i_{opt} is taken at the optimal PSA state $\mathbf{T}_{opt}$ by polarimetric imager. i_{opt}^{com} and i_{opt} can be considered as two different measurements for the same scene, and thus there is a joint relation between them. The probabilities $P(i_{opt})$ and $P(i_{opt}^{com})$ change with i_{opt}^{NN} simultaneously. According to the maximum-likelihood (ML) method [30], the estimator of i_{opt}^{NN} should maximize the joint probability density function $P(i_{opt}) \cdot P(i_{opt}^{com})$, and thus we can get a modified estimator i_{opt}^{our} for i_{opt}^{NN}.

$$\begin{aligned} i_{opt}^{our} &= \arg\max_{i_{opt}^{NN}} \{P(i_{opt}) \cdot P(i_{opt}^{com})\} \\ &= \arg\max_{i_{opt}^{NN}} \{A \exp[B]\}, \end{aligned} \tag{14}$$

where

$$A = \frac{1}{2\pi\,\|C\|\,\sigma^2}, B = -\frac{\left(i_{opt} - i_{opt}^{NN}\right)^2}{2\sigma^2} - \frac{\left(i_{opt}^{com} - i_{opt}^{NN}\right)^2}{2\|C\|^2\sigma^2}, \tag{15}$$

To deduce the closed-form expression of i_{opt}^{our}, one needs to calculate the extremal solution of the joint probability in Eq. (14). Because the joint probability $P(i_{opt}) \cdot P(i_{opt}^{com})$ always increases with the increase of B, i_{opt}^{our} is also the extremal solution of B. By solving equation $dB/di_{opt}^{NN} = 0$, the solution of Eq. (14) can be obtained as:

$$i_{opt}^{our} = \frac{\|C\|^2 i_{opt} + i_{opt}^{com}}{\|C\|^2 + 1}. \tag{16}$$

The mean value and the variance of our estimator i_{opt}^{our} are:

$$\begin{cases} \langle i_{opt}^{our} \rangle = i_{opt}^{NN} \\ Var[i_{opt}^{our}] = \frac{\|C\|^2}{1+\|C\|^2}\sigma^2 \end{cases}. \tag{17}$$

The flowchart of our method can be illustrated more clearly by Fig. 1. Based on the joint relation, the modified image i_{opt}^{our} is derived from traditional optimal image i_{opt} and composite image i_{opt}^{com} which is a combination of measurement images i_1, i_2, i_3, i_4. The essence of the joint relation between i_{opt}

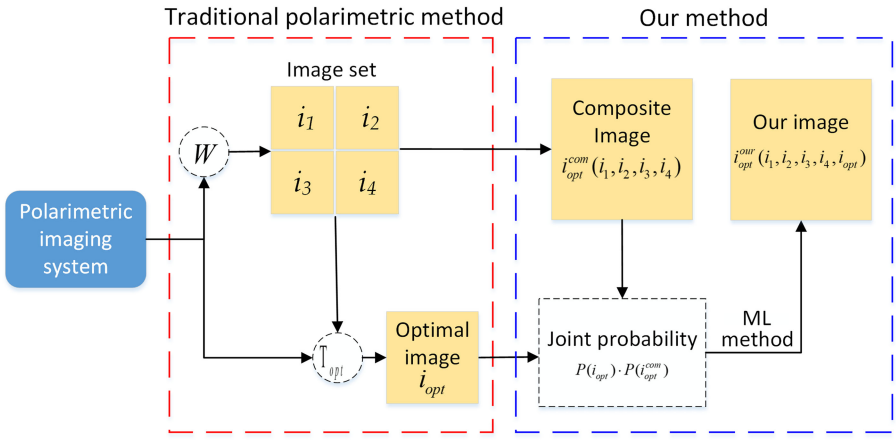

Fig. 1. The flowchart of the joint noise reduction for contrast enhancement in Stokes polarimetric imaging.

and i_{opt}^{com} is that five images (i_1, i_2, i_3, i_4, i_{opt}) describe the scene which has 4-dimensional polarization information. These five images constitute an over-complete set and they are interrelated.

On the other hand, substituting Eqs. (8) and (9) into Eq. (16), the relation between image, measurement matrix W and optimal PSA state $\mathbf{T}_{opt}$ is deduced as:

$$i_{opt}^{our} = \frac{\left\|\mathbf{T}_{opt}^{T}W^{-1}\right\|^2 i_{opt}+2\mathbf{T}_{opt}^{T}W^{-1}(i_1,i_2,i_3,i_4)^T}{\left\|\mathbf{T}_{opt}^{T}W^{-1}\right\|^2+4}. \tag{18}$$

It can be seen from Eq. (18) that i_{opt}^{our} is a linear combination of the five images i_1, i_2, i_3, i_4 and i_{opt}, and the weights of these images are determined by $\mathbf{T}_{opt}$ and W. Generally speaking, the way of combining images shown in Eq. (18) and Fig. 1 is determined by the type of polarimetric parameter, the type of noise and the selection of estimation method. Therefore, the method can be extended to other polarimetric imaging systems, for other types of noise and by different estimation methods.

In order to verify the effect of our method, we introduce the parameter of optimization ratio R as:

$$R = \frac{F\left(i_{opt}^{our}\right)}{F\left(i_{opt}\right)}, \tag{19}$$

where $F(i_{opt}^{our})$ and $F(i_{opt})$ refer to the fisher ratio of the image obtained by our method and the image whose contrast is optimized by traditional polarimetric method. By substituting Eqs. (4), (12) and (17) into Eq. (19), one obtains the expression

$$R = 1+\frac{1}{\|C\|^2}. \tag{20}$$

It is easy to draw a conclusion that R is always greater than one. It means that the image i_{opt}^{our} obtained by our method always has a higher fisher ratio than traditional optimal image i_{opt}. According to Eq. (20), the optimization ratio R is determined by the value of $\|C\|$, which consequently depends on the five states of PSA, $\mathbf{T}_k$, $k = (1, 2, 3, 4)$ and $\mathbf{T}_{opt}$ according to Eq. (1) and (8).

We find that the choice of measurement matrix W can affect the optimization ratio of our method. It can be seen from Eqs. (8) and (20) that R depends on C and C depends on W. The influence of two representative measurement matrices on the optimization ratio R is discussed below.

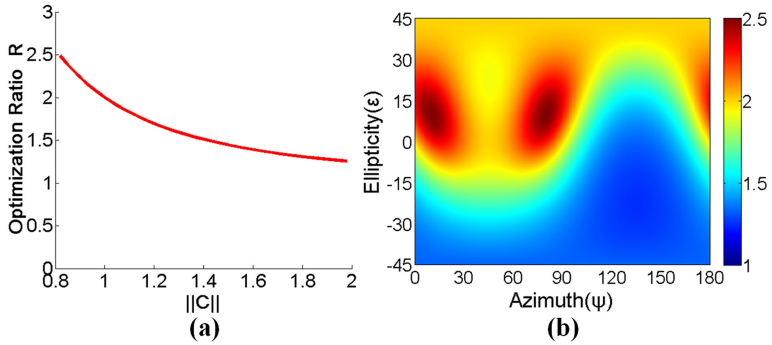

Fig. 2. (a) The variation of the optimization ratio R with $\|C\|$. (b) The variation of the R with the azimuth and ellipticity of $\mathbf{T}_{opt}$.

We consider firstly the measurement matrix of

$$W_1 = \frac{1}{2}\begin{pmatrix} 1 & 1 & 0 & 0 \\ 1 & -1 & 0 & 0 \\ 1 & 0 & 1 & 0 \\ 1 & 0 & 0 & 1 \end{pmatrix}. \tag{21}$$

W_1 is a simply realized measurement matrix that is often adopted in Stokes polarization imaging [31], [32]. In case of W_1, the variation of R with $\|C\|$ can be inferred from Eqs. (8), (20) and (21), as shown in Fig. 2(a). For W_1, according to the numerical simulation with ergodic states of $\mathbf{T}_{opt}$, the range of $\|C\|$ is found to be between 0.8 and 2. According to Eq. (8), the value of $\|C\|$ depends on the traditional optimal PSA state $\mathbf{T}_{opt}$ and thus the relation of R and $\mathbf{T}_{opt}$ can be obtained by substituting W_1 and $\mathbf{T}_{opt}$ into Eqs. (8) and (20). Since $\mathbf{T}_{opt}$ can be expressed by a purely polarized Stokes vector with unit intensity, it has two degrees of freedom: angle of polarization ψ(from 0 to π) and angle of ellipticity ε (from $-\pi/4$ to $\pi/4$) [33]

$$\mathbf{T}_{opt} = (1, \cos 2\psi \cos 2\varepsilon, \sin 2\psi \cos 2\varepsilon, \sin 2\varepsilon)^T \tag{22}$$

and C can be written in the form of:

$$C = \frac{1}{2}(1 + \cos 2\psi \cos 2\varepsilon - \sin 2\psi \cos 2\varepsilon - \sin 2\varepsilon, 1 - \cos 2\psi \cos 2\varepsilon - \sin 2\psi \cos 2\varepsilon - \sin 2\varepsilon, 2 \sin 2\psi \cos 2\varepsilon, 2 \sin 2\varepsilon). \tag{23}$$

Thus, we obtain the relation between R and $\mathbf{T}_{opt}$ with Eqs. (20) and (23). The variation of R with $\|C\|$ and $\mathbf{T}_{opt}$ is shown in Fig. 2. It can be seen that R is always above 1 for any $\|C\|$ and $\mathbf{T}_{opt}$. In particular, when $\mathbf{T}_{opt}$ is taken as $(1, 0.88, 0.32, 0.34)$ or $(1, -0.88, 0.32, 0.34)$, the optimization ratio R reaches the maximum value of 2.5, while when $\mathbf{T}_{opt}$ is taken as $(1, 0, -0.64, -0.77)$, the optimization ratio R reaches the minimum value of 1.3.

The other measurement matrix to discuss for our method is

$$W_2 = \frac{1}{2}\begin{pmatrix} 1 & 1/\sqrt{3} & 1/\sqrt{3} & 1/\sqrt{3} \\ 1 & -1/\sqrt{3} & -1/\sqrt{3} & 1/\sqrt{3} \\ 1 & -1/\sqrt{3} & 1/\sqrt{3} & -1/\sqrt{3} \\ 1 & 1/\sqrt{3} & -1/\sqrt{3} & -1/\sqrt{3} \end{pmatrix}, \tag{24}$$

which is the regular tetrahedron measurement matrix being optimal for minimizing and equalizing the variance of Stokes vector estimation [34]. When W_2 is adopted, we found an interesting fact. By

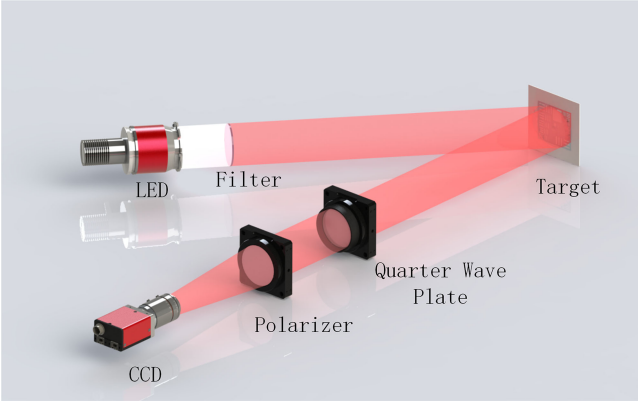

Fig. 3. Schematic of Stokes polarimetric imaging system.

substituting W_2 to Eqs. (8) and (20), it can be deduced that $R \equiv 2$, which means that the optimization ratio R is independent of $\mathbf{T}_{opt}$ and thus the polarization state of the light reflected from the scene. The noise variance is always reduced by half and the fisher ratio of the optimized image is always doubled for any target or background by our method. It also indicates that the optimization ratio will always be the same for any pixel in the image. This consistency makes this method potentially useful in polarimetry.

Furthermore, we generate all the regular tetrahedron measurement matrix by the ergodic method in Ref. [35] and calculate the value of R. We find that $R \equiv 2$, which means that the optimization ratio R is always the same for any regular tetrahedron measurement matrix.

4. Experiments

4.1 Experiments Setup

The schematic of Stokes polarimetric imaging system is shown in Fig. 3. We employ Light-Emitting Diode (Thorlabs, M625L3, 625 nm, 700 mW) together with an optical filter (Daheng Optics, GCC-202004, 633 nm, 10 nm FWHM) to generate the active illumination light with the central wavelength of 633nm. The light reflected from scene passes through the PSA and enters the camera (FLIR, BFS-U3-13Y3, resolution:1280 $\times$ 1024, pixel size: 4.8 μm). The exposure time is set to 10 ms in experiments. The PSA consists of a polarizer (Thorlabs, LPVISE200-A) and a quarter-wave plate (QWP, Thorlabs, WPQ20ME-633, 633 nm). The azimuth angle of polarizer and the fast-axis angle of the QWP are represented by α and β respectively. The regular tetrahedron measurement matrix W_2 given by Eq. (24) is adopted in our experiments for the consistency of optimization. To realize the measurement matrix W_2, the corresponding PSA states represented by the azimuth angle of polarizer and the fast-axis angle of the QWP (α, β) are (40°, 22°), (95°, 22°), (50°, 67°), (140°, 157°).

4.2 Results and Discussions

In order to verify the effect of our method, a simple scene is adopted firstly. The background of the scene is a superposition of a translucent adhesive tape, a film polarizer (Thorlabs, LPVISE2X2) and a piece of white paper. The target is a piece of translucent adhesive tape placed on the background [36]. The optimal image by traditional method (i_{opt}) is shown in Fig. 4(a), and the modified image obtained by our method (i_{opt}^{our}) is shown in Fig. 4(b). By comparing Fig. 4(a) and Fig. 4(b), it can be seen that the intensity fluctuation induced by the noise is considerably lower in Fig. 4(b), which leads to the enhancement of image contrast. In addition, the pixel values along the lines in Fig. 4(a) and Fig. 4(b) are shown in Fig. 4(c) and Fig. 4(d), and it can be seen more clearly that the intensity fluctuation is suppressed by our method. Furthermore, the histograms of I_{opt} and I_{opt}^{our} are also

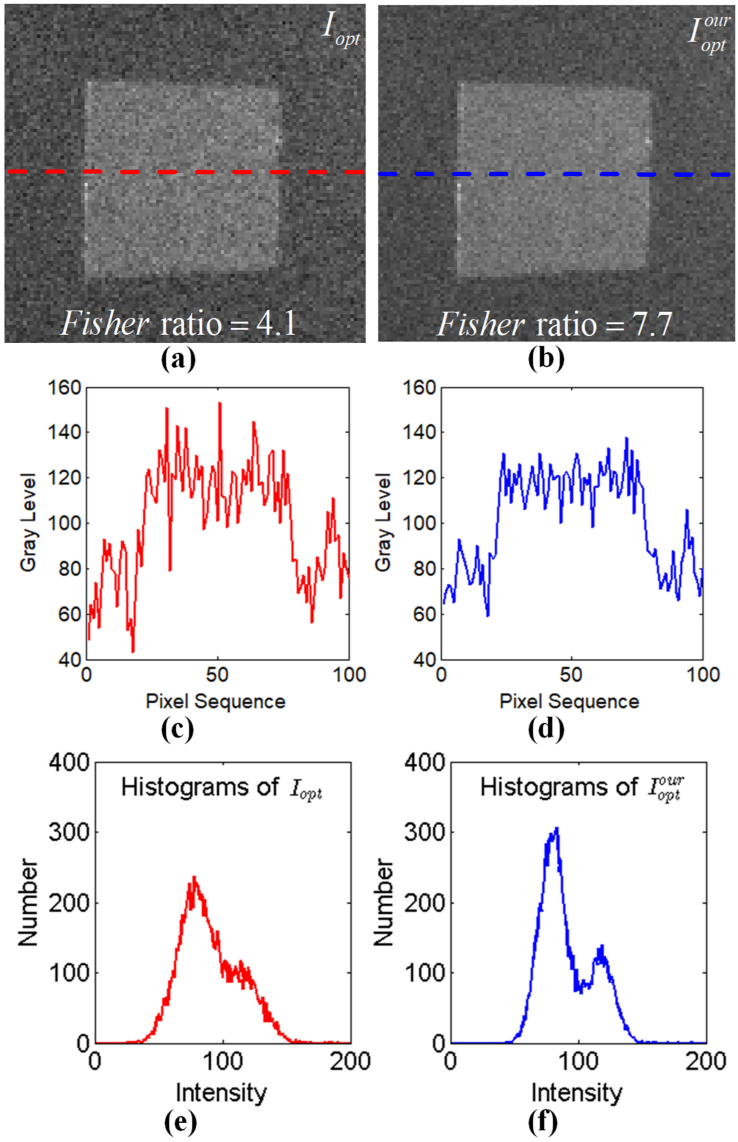

Fig. 4. (a) The contrast optimized image I_{opt} by traditional method. (b) The modified image I_{opt}^{our} by our method. (c) The grey level of the red line in the image I_{opt}. (d) The grey level of the blue line in the image I_{opt}^{our}. (e) The histogram of I_{opt}. (f) The histogram of I_{opt}^{our}.

shown in Fig. 4(e) and Fig. 4(f), and it can be seen that the object and background can also be better discriminated in the histogram of our method.

In order to show the visual effect of our method, another experiment is performed. The target is a metal plate which is hollowed-out according to the 1951 USAF resolution test chart. The background is a white plastic sheet. The Stokes vector of the scattered light in metal region is different from that in plastic region. The optimal image by traditional method and the modified image obtained by our method are shown in Fig. 5. It can be seen that the intensity fluctuation in Fig. 5(b) is lower than that in Fig. 5(a). In particular, in the blue region, a higher spatial resolution can be achieved in Fig. 5(b), and in the red region, the boundary between the target and background is more distinct in Fig. 5(b). The experiment result in Fig. 5 shows that our method can considerably enhance the contrast of the image by reducing the influence of the noise.

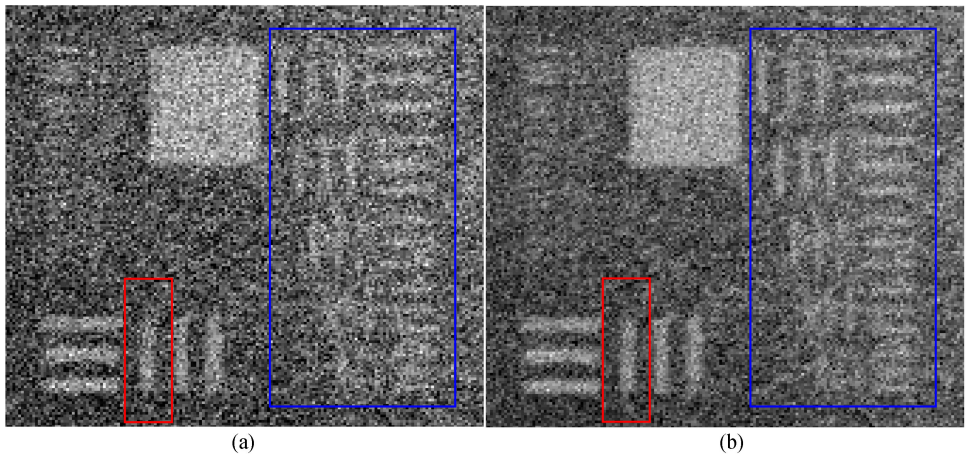

Fig. 5. (a) The contrast optimized image I_{opt} by traditional method. (b) The modified image I_{opt}^{our} by our method.

5. Conclusion

In Stokes polarimetric imaging, the four images captured for calculating the Stokes vector actually contains complete polarization information, and thus can be related to the fifth image captured at the optimal state of PSA. We take advantage of these information to modify the traditional optimal contrast image. Based on the joint relation between the five images taken by polarimetric imager, a method is proposed to obtain the modified image with lower noise and thus higher contrast. The proposed method is an image recovery arithmetic to extract information in polarization image set. Theoretical analysis shows that the image contrast, which is characterized by the fisher ratio, is always improved by our method. In particular, with the regular tetrahedron measurement matrix, it can always decrease the variance by half and double the image contrast in the presence of additive Gaussian noise, and this effect does not depend on the Stokes vectors of the scene. This consistency makes this method potentially useful in polarimetry [26].

In addition, the real-world experiment results are consistent with the theoretical analyses and verify that it is feasible to suppress the disturbance of the noise and thus improve the target/background contrast of the image by our method. It needs to be clarified that, the proposed method is implemented based on the five images which are acquired in the traditional contrast optimization method, and thus the proposed method requires no extra information and does not increase the system complexity. Finally, because the joint relation generally exists in the polarimetric images, the proposed method can be extended to other types of polarimetric imaging system (such as Mueller polarimetric imaging system [8]) and for other types of noise (such as Poisson shot noise [34], [35]).

Acknowledgment

Haofeng Hu acknowledges the Fondation Franco-Chinoise pour la Science et ses Applications (FFCSA) and the China Scholarship Council (CSC).

References

[1] J. S. Tyo, D. L. Goldstein, D. B. Chenault, and J. A. Shaw, "Review of passive imaging polarimetry for remote sensing applications," *Appl. Opt.*, vol. 45, no. 22, pp. 5453–5469, Aug. 1, 2006.
[2] D. J. Diner, A. Davis, B. Hancock, G. Gutt, R. A. Chipman, and B. Cairns, "Dual-photoelastic-modulator-based polarimetric imaging concept for aerosol remote sensing," *Appl. Opt.*, vol. 46, no. 35, pp. 8428–8445, Dec. 10, 2007.
[3] A. A. Kokhanovsky *et al.*, "Space-based remote sensing of atmospheric aerosols: The multi-angle spectro-polarimetric frontier," *Earth-Sci. Rev.*, vol. 145, pp. 85–116, Jun. 1, 2015.

[4] Y. Zhao, L. Zhang, D. Zhang, and Q. Pan, "Object separation by polarimetric and spectral imagery fusion," *Comput. Vis. Image Understanding*, vol. 113, no. 8, pp. 855–866, Aug. 2009.
[5] A. J. Yuffa, K. P. Gurton, and G. Videen, "Three-dimensional facial recognition using passive long-wavelength infrared polarimetric imaging," *Appl. Opt.*, vol. 53, no. 36, pp. 8514–8521, Dec. 20, 2014.
[6] A. Stern, D. Aloni, and B. Javidi, "Experiments with three-dimensional integral imaging under low light levels," *IEEE Photon. J.*, vol. 4, no. 4, pp. 1188–1195, Aug. 2012.
[7] S. L. Jacques, J. C. Ramella-Roman, and K. Lee, "Imaging skin pathology with polarized light," *J. Biomed. Opt.*, vol. 7, no. 3, pp. 329–340, Jul. 2002.
[8] A. Pierangelo *et al.*, "Ex-vivo characterization of human colon cancer by Mueller polarimetric imaging," *Opt. Exp.*, vol. 19, no. 2, pp. 1582–1593, Jan. 17, 2011.
[9] S. L. Jacques, J. R. Roman, and K. Lee, "Imaging superficial tissues with polarized light," *Lasers Surg. Med.*, vol. 26, no. 2, pp. 119–129, 2000.
[10] H. Hu, L. Zhao, B. Huang, X. Li, H. Wang, and T. Liu, "Enhancing visibility of polarimetric underwater image by transmittance correction," *IEEE Photon. J.*, vol. 9, no. 3, Jun. 2017, Art. no. 6802310.
[11] F. Shen, B. Zhang, K. Guo, Z. Yin, and Z. Guo, "The depolarization performances of the polarized light in different scattering media systems," *IEEE Photon. J.*, vol. 10, no. 2, Apr. 2018, Art. no. 3900212.
[12] B. J. Huang, T. G. Liu, H. F. Hu, J. H. Han, and M. X. Yu, "Underwater image recovery considering polarization effects of objects," *Opt. Exp.*, vol. 24, no. 9, pp. 9826–9838, May 2016.
[13] G. Anna, F. Goudail, P. Chavel, and D. Dolfi, "On the influence of noise statistics on polarimetric contrast optimization," *Appl. Opt.*, vol. 51, no. 8, pp. 1178–1187, Mar. 10, 2012.
[14] B. Huang, T. Liu, J. Han, and H. Hu, "Polarimetric target detection under uneven illumination," *Opt. Exp.*, vol. 23, no. 18, pp. 23603–23612, Sep. 7, 2015.
[15] X. Li *et al.*, "Polarimetric image recovery method combining histogram stretching for underwater imaging," *Sci. Rep.*, vol. 8, p. 12430, Aug. 20, 2018.
[16] Y. Y. Schechner, S. G. Narasimhan, and S. K. Nayar, "Polarization-based vision through haze," *Appl. Opt.*, vol. 42, no. 3, pp. 511–525, Jan. 20, 2003.
[17] J. Liang, L. Ren, H. Ju, W. Zhang, and E. Qu, "Polarimetric dehazing method for dense haze removal based on distribution analysis of angle of polarization," *Opt. Exp.*, vol. 23, no. 20, pp. 26146–26157, Oct. 5, 2015.
[18] G. Anna, H. Sauer, F. Goudail, and D. Dolfi, "Fully tunable active polarization imager for contrast enhancement and partial polarimetry," *Appl. Opt.*, vol. 51, no. 21, pp. 5302–5309, Jul. 20, 2012.
[19] F. Goudail and M. Boffety, "Optimal configuration of static polarization imagers for target detection," *J. Opt. Soc. Amer. A*, vol. 33, no. 1, pp. 9–16, Jan. 1, 2016.
[20] F. Goudail and A. Beniere, "Optimization of the contrast in polarimetric scalar images," *Opt. Lett.*, vol. 34, no. 9, pp. 1471–1473, May 2009.
[21] M. Richert, X. Orlik, and A. D. Martino, "Adapted polarization state contrast image," *Opt. Exp.*, vol. 17, no. 16, pp. 14199–14210, Aug. 2009.
[22] A. Peinado, A. Lizana, J. Vidal, C. Iemmi, and J. Campos, "Optimization and performance criteria of a Stokes polarimeter based on two variable retarders," *Opt. Exp.*, vol. 18, no. 10, pp. 9815–9830, May 10, 2010.
[23] Q. Yan *et al.*, "Cross-field joint image restoration via scale map," in *Proc. IEEE Int. Conf. Comput. Vis.*, 2013, pp. 1537–1544.
[24] F. E. Turkheimer, N. Boussion, A. N. Anderson, N. Pavese, P. Piccini, and D. Visvikis, "PET image denoising using a synergistic multiresolution analysis of structural (MRI/CT) and functional datasets," *J. Nucl. Med.*, vol. 49, no. 4, pp. 657–666, Apr. 2008.
[25] L. Xiang, Y. Qiao, D. Nie, L. An, Q. Wang, and D. Shen, "Deep auto-context convolutional neural networks for standard-dose PET image estimation from low-dose PET/MRI," *Neurocomputing*, vol. 267, pp. 406–416, Dec. 6, 2017.
[26] X. Li, T. Liu, B. Huang, Z. Song, and H. Hu, "Optimal distribution of integration time for intensity measurements in Stokes polarimetry," *Opt. Exp.*, vol. 23, no. 21, pp. 27690–27699, Oct. 19, 2015.
[27] M. R. Foreman, A. Favaro, and A. Aiello, "Optimal frames for polarization state reconstruction," *Phys. Rev. Lett.*, vol. 115, no. 26, Dec. 31, 2015, Art. no. 263901.
[28] K. Fukunaga, *Introduction to Statistical Pattern Recognition*. New York, NY, USA: Academic, 1990.
[29] T. Mu, Z. Chen, C. Zhang, and R. Liang, "Optimal design and performance metric of broadband full-Stokes polarimeters with immunity to Poisson and Gaussian noise," *Opt. Exp.*, vol. 24, no. 26, pp. 29691–29704, Dec. 26, 2016.
[30] H. Hu, G. Anna, and F. Goudail, "On the performance of the physicality-constrained maximum-likelihood estimation of Stokes vector," *Appl. Opt.*, vol. 52, no. 27, pp. 6636–6644, Sep. 20, 2013.
[31] X. Li, H. Hu, L. Wu, and T. Liu, "Optimization of instrument matrix for Mueller matrix ellipsometry based on partial elements analysis of the Mueller matrix," *Opt. Exp.*, vol. 25, no. 16, pp. 18872–18884, Aug. 7, 2017.
[32] S. X. Wang and A. M. Weiner, "Fast wavelength-parallel polarimeter for broadband optical networks," *Opt. Lett.*, vol. 29, no. 9, pp. 923–925, May 1, 2004.
[33] D. Goldstein, *Polarized Light*. New York, NY, USA: Marcel Dekker, Inc., 2003.
[34] F. Goudail, "Noise minimization and equalization for Stokes polarimeters in the presence of signal-dependent Poisson shot noise," *Opt. Lett.*, vol. 34, no. 5, pp. 647–649, Mar. 2009.
[35] G. Anna and F. Goudail, "Optimal Mueller matrix estimation in the presence of Poisson shot noise," *Opt. Exp.*, vol. 20, no. 19, pp. 21331–21340, Sep. 2012.
[36] M. Boffety, H. Hu, and F. Goudail, "Contrast optimization in broadband passive polarimetric imaging," *Opt. Lett.*, vol. 39, no. 23, pp. 6759–6762, Dec. 1, 2014.